Dye Lasing and Planar Extensional Flow Induced Dissolution in Hydrodynamically Trapped Microdroplets

A dissertation submitted in partial satisfaction of the
requirements for the degree of

Master of Science

in

Optoelectronics and Photonics Engineering

by

Oğuz Kayıllıoğlu

Koç University

September 2015

Koç University
Graduate School of Sciences and Engineering

This is to certify that I have examined this copy of a master's thesis by

Oğuz Kayıllıoğlu

and have found that it is complete and satisfactory in all respect
and that any and all revisions required by the final
examining committee have been made.

Committee Members:

Alper Kiraz, Ph.D. (Advisor)

Melikhan Tanyeri, Ph.D.

Metin Muradoğlu, Ph.D.

September 2015

Dye Lasing and Planar Extensional Flow Induced Dissolution in Hydrodynamically Trapped Microdroplets

Copyright 2015
by
Oğuz Kayıllıoğlu

Acknowledgements

First, I would like to thank my advisor Alper Kiraz and co-advisor Melikhan Tanyeri for their support. Second, I would like to thank Dr. Ahmet Erten for his advices on production of microfluidic chips. Third, I would like to thank to Metin Muradoğlu for leading us finding an approriate theoretical equation modelling the dissolution. Forth, I am thankful to Ph.D. student Muhammed Irfan for his help on solving the dissolution equation. Fifth, I would like to thank Ph.D. student Mustafa Eryürek at Optofluidics and Nano-optics Laboratory for his help on characterization of microfluidic molds.

Last, I would like to thank to Koç University Seed Research Program.

Curriculum Vitae
Oğuz Kayıllıoğlu

Personal	Born in July 18, 1989, Bursa, Turkey
Education	
09/2013-09/2015	M.S. Optoelectronics-Photonics Engineering, Koç University, Istanbul Dissertation: Dissolution of Hydrodynamically Trapped Liquid Microdroplets in Planar Extensional Flow
02/2012-06/2013	B.S. in Electrical-Electronics Engineering, Koç University, Istanbul
09/2007-06/2013	B.S. in Physics, Koç University, Istanbul
Work Experince	
09/2013-presenet	Research Assistant, Koç University Optofluidics and Nano-photonics Laboratory
09/2013-present	Teaching Assistant, Koç University General Physics-1, Fall 2013, Fall 2014 General Physics-2, Spring 2015 General Physics-4, Spring 2014
Internship	
June 2012	Bosch Plant, Bursa
July 2012	ING Bank, Istanbul
Publications & Presentations	A. Kiraz, O. Kayillioglu, A. Erten, and M. Tanyeri, "Dye Lasing and Laminar Flow-Induced Dissolution in Hydrodynamically Trapped Oil Microdroplets," in Optics in the Life Sciences, OSA Technical Digest (online) (Optical Society of America, 2015), paper OtW2D.

ABSTRACT

Dye Lasing and Planar Extensional Flow Induced Dissolution in Hydrodynamically Trapped Microdroplets

by

Oğuz Kayıllıoğlu

Dissolution of one phase into an immiscible phase is of great importance to food and drug industry. Dissolution process is mainly affected by diffusion coefficient, solubility, density and viscosity of the dissolving material in the immiscible phase. This thesis reports dye lasing in hydrodynamically manipulated microdroplets and proposes the hydrodynamic trap as a new method to observe dissolution of microdroplets.

In the first part of this thesis, utilizing previously available hydrodynamic trapping method, we trap and manipulate the position of a dye doped liquid microdroplets in a microfluidic chip. By manipulating the position of the trapped droplets along the outlet channels of the microfluidic chip, we show lasing can be achieved for different positions of the droplet. When a trapped microdroplet is excited at a fixed position, lasing modes in the consecutive spectra of the droplet show a blue shift for all modes. The shift in modes is an indicator of the dissolution. Therefore, the next part focuses on dissolution of liquid microdroplets.

Within a microfluidic chip, a trapped liquid microdroplet is exposed to planar extensional flow which increases the rate of the mass transfer out of the microdroplet. The static dissolution, that is diffusion, of droplets is modelled by Epstein and Plesset. However, the hydrodynamic trap induces flow around a trapped particle, therefore besides diffusion, the effect of convection should also be considered.

The change in particle's radius as a function of time in the presence flow is numerically investigated by Zhang et al. To fit the experimental data we use the model provided by Zhang.

The liquids used in the microdroplet dissolution experiments were n-octanol, n-decanol, undecanol and benzyl benzoate. Benzyl Benzoate and n-octanol showed good agreement with the Zhang model. In addition, experiments revealed that concentration of surfactant is an important parameter affecting dissolution rate which requires further investigation.

ÖZET

Düzlemsel Genişlemeli Akış İçinde Hidrodinamik Tuzaklanmış Mikrodamlaların Işıması ve Çözülmesi

Karışmayayan iki fazın birbiri içinde çözülmesi yemek ve ilaç sanayisi için önemli bir problemdir. Çözülme prosesini etkileyen temel faktörler difüzyon katsayısı, çözünürlük, özkütle ve viskositedir. Bu tez hidrodinamik tuzaklanıp hareket ettirilen mikdrodamlaların ışımasını raporlar. Bunun yanında kullanılan hidrodinamik tuzaklama yöntemini mikrodamlaların çözülmesini incelemek için yeni bir metot olarak sunar.

Tezin ilk kısmında, hidrodinamik tuzakla hareket ettirilen boyanmış mikrodamların, uygun dalga boyundaki bir lazer ışığıyla uyarılınca, farklı modlarda lazer ışığı ürettiğini gösteriyoruz. Bunun yanında tuzakladığımız mikroküreyi aynı konumda art arda uyarınca, ışıma modlarının kısa dalga boylarına kaydığını gözlemledik. Bu kayma tuzaklanan mikrodamlanın zaman içerisinde çözülüp yarı çapının azaldığına işaret etmektedir. İkinci kısım bu çözülmeyi farklı malzemeler için gözlemlemek ve modellemeye çalışmaktır.

Mikrofluidik çip içerisinde tuzaklanan sıvı damlaları, genişlemeli akışa maruz kalırlar ve bu akış damlaların çözülmesini hızlandırır. İçinde akış bulunmayan sıvı içerisine bırakılan gaz kürelerinin çözülmesi Epstein ve Plesset tarafından modellenmiştir. Bizim durumuzda ise konveksiyon etkisini Epstein-Plesset denklemine dahil eden yeni bir modele ihtiyaç vardır. Zhang modeli dediğimiz bu model literatürden bulunup, mevcut sisteme uygulanmıştır.

Kullanılan sıvılar n-octanol, n-decanol, undecanol ve benzyl benozate'dır. Bu kimyasalları seçmemizin en önemli nedeni çözülmeyi etkileyen, difüzyon katsayısı,

çözünürlük, viskosite ve özkütle gibi değerlerinin, literatürde ölçülmüş olmasından ya da hesaplanış olmasından ileri gelmektedir. Yaptılan ölçümlerin bir bölümü kullanılan modele uyum göstermektedir. Bununla birlikte yapılan deneyler, kullanılan yüzey aktif madde konsantrasyonunun çözülmeye olan etkisini ortaya çıkartmıştır.

Contents

1 Introduction **15**

2 Dye Lasing and Laminar Flow-Induced Dissolution in Hydrodynamically Trapped Oil Microdroplets **19**

2.1 Lasing from a Manipulated Microdroplet 20

2.2 Laminar Flow-Induced Dissolution of Benzyl Benzoate Microdroplets 21

3 Dissolution of Hydrodynamically Trapped Microdroplets in Planar Extensional Flow **25**

3.1 Dissolution of n-Octanol Microdroplets 25

3.2 Dissolution of Benzyl Benzoate Microdroplets 27

3.3 The Effect of the Surfactant Concentration on the Dissolution of Benzyl Benzoate and n-Octanol Microdroplets 29

3.4 Dissolution of n-Decanol and Undecanol Microdroplets 31

4 Oscillation Analysis of a Hydrodynamically Trapped Benzyl Benzoate Microdroplet **33**

5 Modelling **35**

5.1 The Epstein-Plesset Model 35

5.2 The Kurdyumov-Polyanin-Zhang Model 38

6 Experimental Setup **45**

6.1 Microfluidic Chip and Fabrication 46

6.2 Experimental Setup for Dye Lasing in Hydrodynamically Trapped Microdroplets 49

6.3 Microdroplet Generation and Injection 50
6.4 Image Analysis 51
6.5 Physical Properties of the Materials 51

7 Conclusion & Discussion **53**

8 Appendix A **55**

List of Figures

1 Dye lasing from a hydrodynamically manipulated benzyl benzoate microdroplet. Figure (A) shows lasing spectrum at the initial position of the microdroplet and Figure (B) shows lasing spectrum at the final position. 20

2 The position of a lasing peak from a consecutive spectra as a function of time 22

3 Change in the radius of a microdroplet in the absence and presence of extensional flow 23

4 Dissolution of an n-Octanol droplet at flow rates 10 and 20 μl/h. . . 26

5 Dissolution of a benzyl benzoate microdroplet at 10 μl/h. 27

6 Dissolution of a benzyl benzoate microdroplet at 20 μl/h. 28

7 Dissolution of a benzyl benzoate microdroplet in water at 10 mM surfactant concentration 29

8 Dissolution of a n-octanol microdroplet in water at 10 mM surfactant concentration 30

9 Dissolution of a n-decanol microdroplet in water at 10 μM surfactant concentration. 31

10 Dissolution of an undecanol microdroplet in water at 10 μM surfactant concentration 32

11 Position of a hydrodynamically trapped microdroplet on the y-axis. 33

12 Power spectral density of the position on the y-axis of a hydrodynamically trapped microdroplet. 34

13 The framework of the hydrodynamic trap setup 45

14 Layout of the microfluidic chip 47
15 A hydrodynamically trapped benzyl benzoate droplet in extensional flow 48
16 Pneumatic membrane valve showing the effect of applied pressure. . 49
17 Experimental setup for dye lasing. 50

List of Tables

1 Materials used in the experiments; three alcohols and benzyl benzoate with measured saturation concentrations and calculated diffusion coefficients. 52

NOMENCLATURE

Q	Quality Factor
WGM	Whispering Gallery Modes
DSS	Docusate Sodium Salt
λ	Wavelength
r	Radius
r_0	Initial Radius
c	Unitless Concentration
c_i	Initial Concentration
c_s	Saturation Concentration
D	Diffusion Coefficient
K	Mass Transfer Coefficient
U	Free Stream Velocity
ρ	Density
Sh	Sherwood Number
Pe	Peclet Number
β	Viscosity Ratio

1 Introduction

Microfluidics is an interdisciplinary science emerged in 1980s which explains how fluids behave at the micro scale. It is popularized because it enables high performance, low cost, rapid processing of liquids at the microscale. These processes include mixing [1, 2], liquid separation [3], cell separation [4], macromolecule separation [5] droplet generation [6], DNA replication [7] and so on. The volume of the fluid used in microfluidic application ranges from micro to femtoliters. One of the common methods to fabricate microfluidic devices is casting PDMS(Polydimethysiloxane) on a silicon wafer. PDMS is an organic polymer which is extensively used due to its versatile characteristics such as optical transparency and inertness. Typical components used in a microfluidic setup include PDMS chip with valves, tubing, connectors, syringes, syringe pumps and so on.

For the last 30 years, numerous noncontact methods have been demonstrated for trapping micro/nano-particles using forces generated by optical, electrical, acoustic, and acoustic potential fields [8, 9, 10]. Despite the versatility of these methods, new approaches are still needed for confinement and observation of objects with arbitrary shapes for studies in protein folding, single polymer dynamics, or single cell mechanics. Recently, hydrodynamic trapping has been introduced as a powerful tool for trapping and manipulation of microbeads, DNA molecules, and cells [11, 12, 13]. Hydrodynamic trapping is a confinement method that only requires fluid flow to trap particles. This thesis reports, based on hydrodynamic trapping of liquid microdroplets in a microfluidic chip, dye lasing in trapped microdroplets and also proposes the hydrodynamic trapping as a novel method for measuring diffusion coefficient and solubility of the trapped microdroplets.

The trapped microdroples which are liquid microspheres, can naturally serve as optical microcavities hosting high quality whispering gallery modes, thanks to their self-organized spherical shape and smooth surface dictated by the surface tension of the liquid. These properties are prerequisite for low-threshold lasing which is of great importance for integrated tunable organic light sources. Previously, it has been shown that lasing in dye-doped microdroplets of immersion oil emulsified in water that are manipulated by a single beam optical trap [14]. In this thesis, we extend the previous study to lasing in dye-doped microdroplets of benzyl benzoate emulsified in water which are trapped and manipulated by a hydrodynamic trap in a planar extensional flow.

The dissolution of liquid microdroplets in aqueous solutions has been a research interest for a long time. It is particularly important for drug and food industry. One parameter characterizing the dissolution is diffusion coefficient. Diffusion coefficient is an important parameter for industrial applications such as separation processes and drug delivery/design [15, 16].

There are numerous techniques to measure the diffusion coefficient of a liquid in another solution. One typical examples employs Taylor-Aris dispersion [17, 18]. This method utilizes a slowly flowing solvent in a tube and introduction of a δ shaped solute into the tube. As the solute moves along the tube, due to both flow and diffusion, there is dispersion of the solute in both the axial and the radial direction. The parabolic flow profile in the tube increases the diffusion rate in the radial direction. By the theoretical study of Taylor and Aris, concentration distribution and the effective diffusion coefficient of the solute along the radial direction can be calculated. Another method for measuring diffusion coefficients utilizes diaphragm cells [19]. In this technique there are two adjacent chambers

separated by a diaphragm cell filled with different liquids. After diffusion of the materials into the chambers, concentration of the materials in both chambers are measured and diffusion coefficient is calculated with reference to a calibration system. Less common and relatively new techniques include NMR pulse gradient [20] and surface plasmon resonance [21]. But these techniques aren't suitable for measuring the diffusion coefficients of liquid droplets.

Theoretically, dissolution of gas bubbles in liquid-gas solutions is studied by Epstein and Plesset [22]. They provided an equation modelling the change in a gas bubble radius as a function of time in an ambient host fluid. Recently, dissolution of gas microbubbles in aqueous media has been experimentally studied with high accuracy. Duncan and Needham formed gas microbubbles using a unique micro manipulation technique and observed them in the absence of flow in the ambient host fluid [23]. This technique utilizes a micropipette to form individual gas microbubbles. They were able to study these individual gas bubbles under various concentrations of the ambient host fluid and proved the Epstein-Plesset model to be accurate.

The same group utilized the micropipette technique to observe single liquid microdroplet dissolution in water and showed that the Epstein-Plesset model successfully explains the dissolution of liquid microdroplets in a second phase medium [24]. Later, they modelled the mass transfer out of a multicomponent liquid droplet in an immiscible environment. Using a similar experimental setup, Su et.al. studied the mass transfer out of mixed droplets of amly, buthyl and ethyl acetate in water environment [25] and measured the diffusion coefficients of these materials. They modified the Epstein-Plesset equation by a scalar, that is the area fraction of the specific component in a microdroplet, incorporating the effect of individual

materials to the dissolution process. In terms of flow conditions, this study was identical to the previous studies except dissolving droplets were multicomponent.

In this study, we extend the previous work using the micropipette technique to dissolution of a microdroplet into a second phase solvent using the hydrodynamic trapping of liquid microdroplets. The single component droplet materials used in the experiments were n-octanol, n-decanol, undecanol and benzyl benzoate. This dissolution measurement technique differs from previous methods in terms of flow conditions. Since droplets are trapped at the stagnation point of two opposing planar extensional creeping flows, the dissolution process is faster than no flow case and consequently this method can be used for quantifying dissolution of droplets in an ambient host fluid in shorter time periods.

In order to incorporate the effect of flow in an ambient host fluid in which a droplet is dissolving, the convection-diffusion equation must be solved. The numerical solution of the axisymmetric mass transfer problem for spherical particles, drops and bubbles in linear Stokes shear flow is studied by Kurdyumov and Polyanin [26] and they proposed simple approximate expressions for Sherwood number which is defined as the ratio of the total mass transport to the diffusive mass transport. Recently, Zhang et al. [27] has done the first detailed numerical investigation on the mass transfer outside a solid or liquid sphere immersed in a simple extensional flow for larger range of Peclet compared to the study by Kurdyumov and showed the approximate correlations are valid. In this thesis, we use the Kurdyumov-Polyanin-Zhang model to calculate change in droplet radius as a function of time and compare it with the experimental data.

2 Dye Lasing and Laminar Flow-Induced Dissolution in Hydrodynamically Trapped Oil Microdroplets

The first part of the thesis is dedicated to manipulation and lasing in hydrodynamically trapped liquid microdroplets. Droplets take almost spherical shape, thereby yielding a high quality Q factor optical resonator capable of hosting whispering gallery modes (WGMs). Previously it has been shown dye lasing in optically manipulated microdroplets [14] and this study extends the previous one to dye lasing in hydrodynamically manipulated microdroplets. In this work, microdroplets are trapped in a glycerol-water solution to keep the droplets buoyant.

The emulsion system selected for the study is dye doped benzyl benzoate microdroplets and the microdroplets are dispersed in a host liquid of 50 % glycerol-water at 10mM surfactant concentration of Docusate Sodium Salt(DSS). This configuration of the experimental setup ensures density matching while keeping high refractive index difference between the host fluid and benzyl benzoate microdroplets. Whispering gallery modes are sustained within microdroplets with minimum buoyancy effects thereby facilitating hydrodynamic trapping. DiI(3) (1,10-Dioctadecyl-3,3,3',3'-tetramethylindo carbocyanine perchlorate, Sigma Aldrich) is used as the gain medium for lasing droplets, which has a hydrophilic chromophore and a hydrophobic side chain. Due to the hydrophilic and hydrophobic chains, DiI(3) resides at benzyl benzoate and glycerol-water interface hence DiI(3) is well suited for efficient pumping of WGMs. The microdroplets are generated by vigorous mechanical agitation of a two phase fluid consisting of benzyl benzoate and

water.

2.1 Lasing from a Manipulated Microdroplet

A trapped microdroplet is optically pumped by a homemade Q-switched $Nd : YVO_4$ laser (20 ns pulse-width, 33 kHz repetition rate, maximal average output power 20 mW) at $\lambda = 532$ nm. A microscope objective with 20x magnification and 0.4 numerical aperture was used for imaging the trapped droplet under bright field, to deliver the laser beam and to collect the emission signal from the lasing droplet. Lasing emission from the dye doped microdroplets were recorded by a spectrometer with a monochromator (500mm; Acton Research) and a CCD detector (Pixis 100; Princeton Instruments). Figure 1 shows lasing from a hydrodynamically manipulated microdroplet.

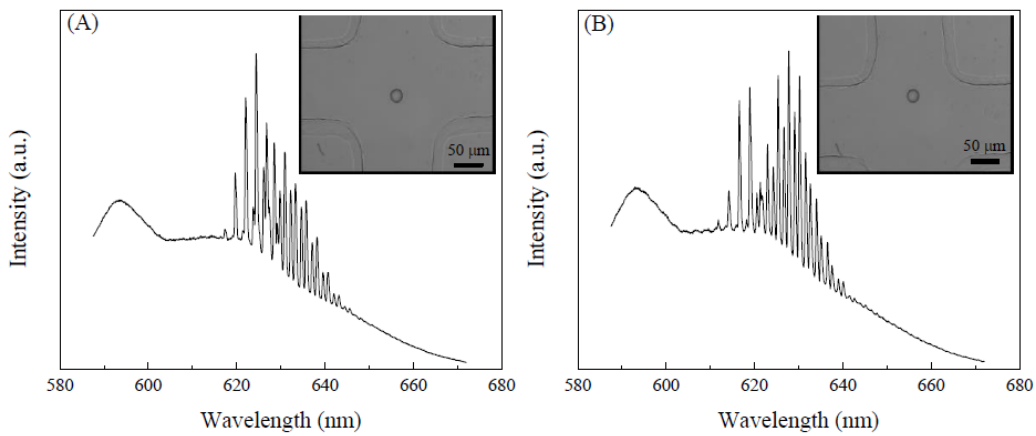

Figure 1: Dye lasing from a hydrodynamically manipulated benzyl benzoate microdroplet. Figure (A) shows lasing spectrum at the initial position of the microdroplet and Figure (B) shows lasing spectrum at the final position.

The dye lasing experiments of the hydrodynamically trapped microdroplets

revealed dissolution of the microdroplets in ambient host fluid. At a fixed position of a microdroplet, consecutive lasing spectra shows a blue shift. Following subsection quantifies the blue shift.

2.2 Laminar Flow-Induced Dissolution of Benzyl Benzoate Microdroplets

The experiments showed substantial dissolution of benzyl benzoate microdroplets in glycerol-water solution in the presence of simple extensional flow. This was revealed by the shift in the peak wavelengths of the lasing modes in the consecutive spectra from a single droplet at a fixed position. Figure 2 shows the shift in a lasing peak from the consecutive spectra of a benzyl benzoate microdroplet at 10 μl/h flow rate.

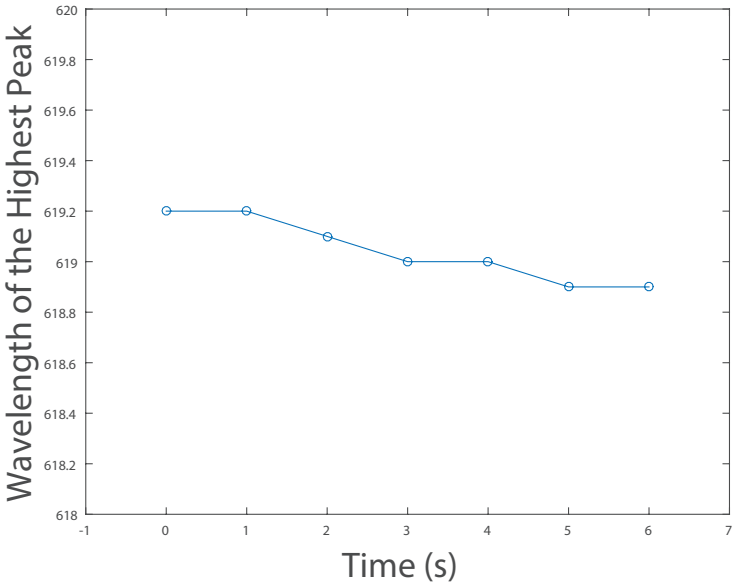

Figure 2: The position of a lasing peak from a consecutive spectra as a function of time

The previous experiment allowed us to observe dissolution from lasing spectra within a few seconds. To see the dissolution for longer time periods, we observed the trapped microdroplets for 30 minutes and recorded images. Figure (3) shows the normalized variation in the radius of two different microdroplets as a function of time at different flow rates. The first microdroplet is observed in water where there is no flow and second microdroplet is observed in the hydrodynamic trap.

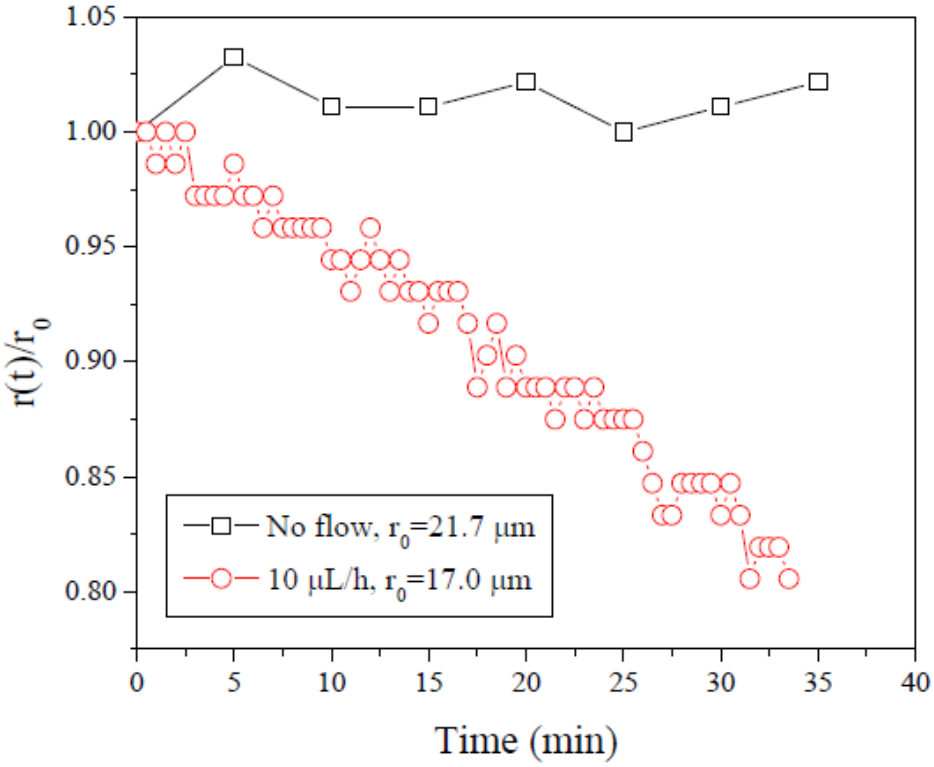

Figure 3: Change in the radius of a microdroplet in the absence and presence of extensional flow

The red data points in Figure 3 are recorded from a hydrodynamically trapped microdroplet at 10 μl/h flow rate and the black data points are taken from a microdroplet in a quiescent ambient host fluid. In the absence of flow in the host fluid, microdroplet radius indicates no discernible variation for a period of 35 minutes. In contrast, for a hydrodynamically trapped microdroplet, we observed 10% reduction in the microdroplet radius within approximately 20 minutes. This experiment raises questions of how fast a hydrodynamically trapped microdroplet dissolves over time in planar extensional flow? What are the contributing factors

to dissolution? How the material properties and flow conditions of an ambient host fluid affect the dissolution process? The theoretical basis of the dissolution of droplets in a quiescent ambient host fluid and in simple extensional flow is going to be discussed in the next section.

3 Dissolution of Hydrodynamically Trapped Microdroplets in Planar Extensional Flow

3.1 Dissolution of n-Octanol Microdroplets

To investigate the effect of the flow rate on the dissolution process, we trapped single microdroplets of various materials at two different flow rates. Figure (4) shows the experimental results and theoretical models for dissolution of hydrodynamically trapped n-octanol microdroplets. It was the fastest dissolving material among other alcohols and benzyl benzoate due to its high solubility. Since we left sample fluid valve open, after some time, only fully saturated sample fluid without droplets is injected. For this specific configuration, a microdroplet is trapped with 1 unit volume of the unsaturated host fluid coming from the right inlet, 1 unit volume of the unsaturated host fluid coming from the left inlet and 2 unit volumes of the saturated sample fluid coming from the right inlet. First, we used 5 μl/h flow rate. This flow rate is injected into the chip from both the host fluid and the sample fluid. Effective the flow rate of the fluid was 10 μl/h in the channel with 50% octanol concentration.

The other flow rate tested is 10 μl/h. As stated above, effective flow rate is twice the pump rate therefore for this experiment, we have a host fluid at 20 μl/h flow rate at 50% n-octanol concentration. Figure 4 shows our results for the experimental data and the modelling equations.

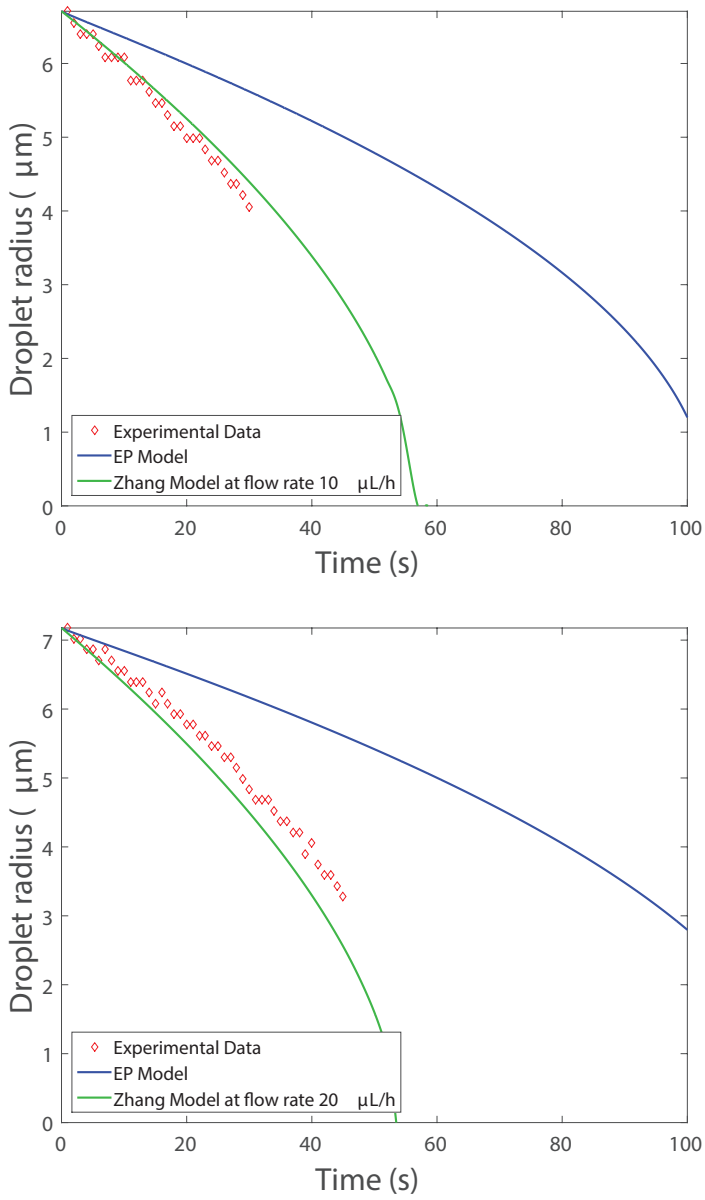

Figure 4: Dissolution of an n-Octanol droplet at flow rates 10 and 20 μl/h.

We see a nearly perfect fit of the modelling equation to the experimental data both for 10 μl/h and 20 μl/h flow rates. These results show accuracy of the Zhang-Kurdyumov-Polyanin model for both flow rates. In the analysis of the ex-

perimental data, even though the unsaturated host fluid doesn't mix perfectly with the saturated host fluid, we assumed host solution at 50% octanol concentration.

In addition, we observed the dissolution of benzyl benzoate microdroplets. Next section reports the dissolution of hydrodynamically trapped benzyl benzoate microdroplets.

3.2 Dissolution of Benzyl Benzoate Microdroplets

Here we worked with a pure host fluid, DI water, without any droplet material concentration in it unlike n-octanol dissolution experiments. Figure 5 and 6 shows the experimental data and the modelling equations for the dissolution of benzyl benzoate.

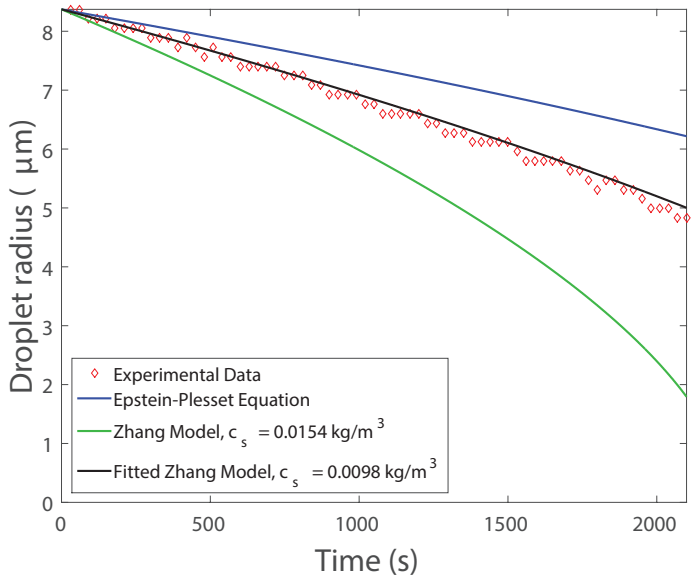

Figure 5: Dissolution of a benzyl benzoate microdroplet at 10 μl/h.

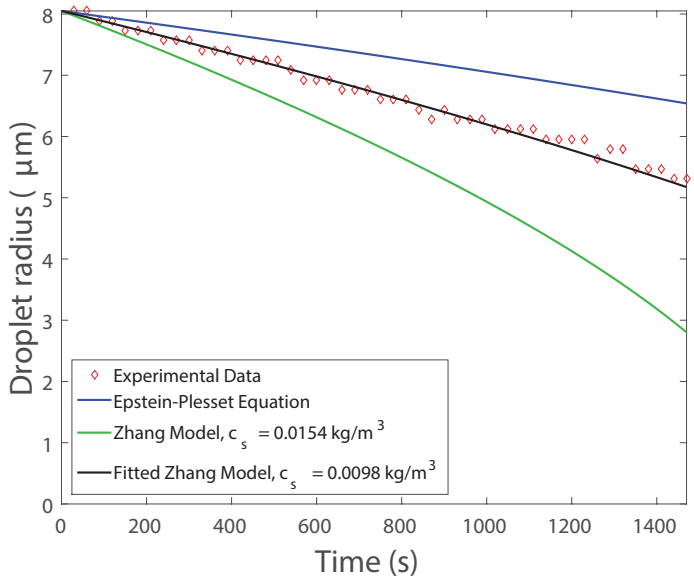

Figure 6: Dissolution of a benzyl benzoate microdroplet at 20 μl/h.

Figure 5 displays that the experimental data falls between the Epstein-Plesset and the Zhang-Kurdyumov-Polyanin models. We explain this discrepancy with the difference in the actual solubility and provided solubility of benzyl benzoate. To fit our experimental data to the Zhang-Kurdyumov-Polyanin model, the solubility value is left as a free parameter and then the fitted solubility was calculated to be 0.0098 kg/m^3.

To investigate validity of the model further, we tried the other flow rate that is 20 μl/h. Figure 6 graphs the dissolution of a benzyl benzoate microdroplet at 20 μl/h flow rate. Here again the experimental data falls between two modelling equations. By setting solubility as the only free parameter in the Zhang model, we calculate the fitted solubility to be 0.0098 kg/m^3 again. These experiments are repeated for 3 different microdroplets at each flow rate and the results showed good consistency in the fitted solubility parameter.

The following section reports the effect of surfactant concentration on dissolution of n-octanol and benzyl benzoate microdroplets.

3.3 The Effect of the Surfactant Concentration on the Dissolution of Benzyl Benzoate and n-Octanol Microdroplets

To investigate the effect of the surfactant concentration on the dissolution rate, we repeated the experiments at flow rate 10 μl/h both for benzyl benzoate and n-octanol microdroplets.

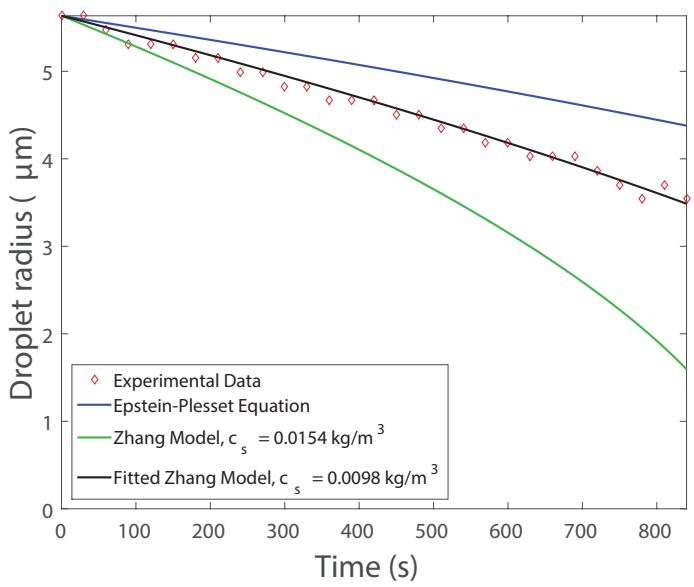

Figure 7: Dissolution of a benzyl benzoate microdroplet in water at 10 mM surfactant concentration

In Figure 7 the same fitting parameter which is solubility is used. At this specific surfactant concentration, the rate of the dissolution of benzyl benzoate

microdroplets isn't different than the the case where surfactant concentration was 10μM. However, this trend is not valid for the dissolution of n-octanol. Figure 8 shows the effect of the surfactant concentration on the dissolution of n-octanol microdroplets.

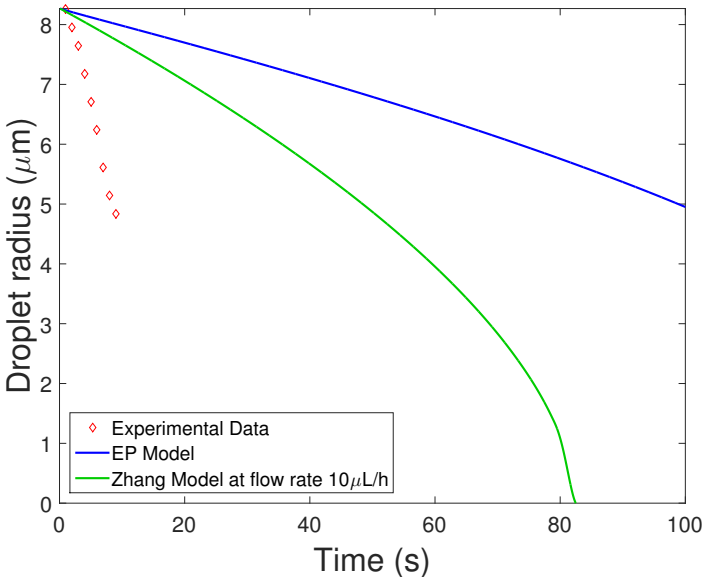

Figure 8: Dissolution of a n-octanol microdroplet in water at 10 mM surfactant concentration

The rate of dissolution of n-octanol microdroplet is greatly enhanced by increase in surfactant concentration. Apparently, the concentration of the surfactant is not in the model as a parameter. Therefore, the model should be revised. Also Zhang model assumes that change in the droplet radius is slow that it doesn't effect the transport process. However, this is not a valid assumption anymore for the dissolution of n-octanol microdroplets in water at 10mM surfactant concentration since the dissolution takes place within a short amount of time ($<$ 1 minute).

3.4 Dissolution of n-Decanol and Undecanol Microdroplets

This section shows the dissolution of n-decanol and undecanol microdroplets. Dissolution graphs of n-decananol and undecanol doesn't fit to our experimental results. These results imply one or more of the parameters effecting the dissolution is different from the values provided in the literature. Figure 9 displays the dissolution of an n-decanol droplet at 10 μl/h.

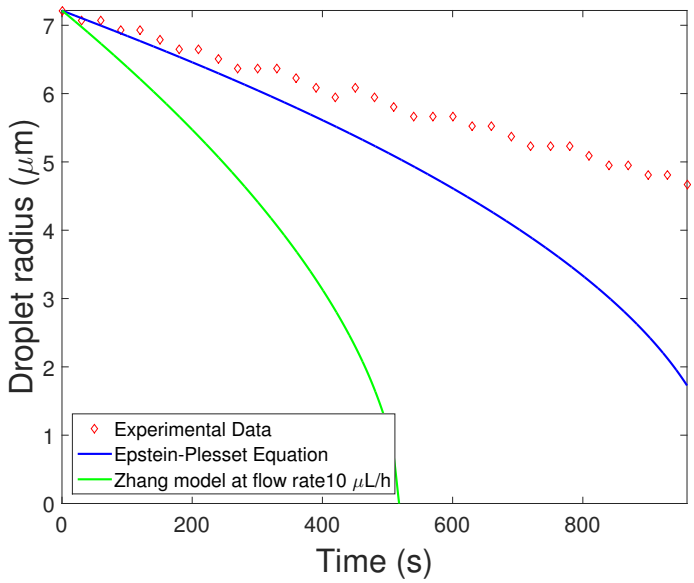

Figure 9: Dissolution of a n-decanol microdroplet in water at 10 μM surfactant concentration.

Figure 10 displays the dissolution of an undecanol microdroplet at 10 μl/h flow flow rate.

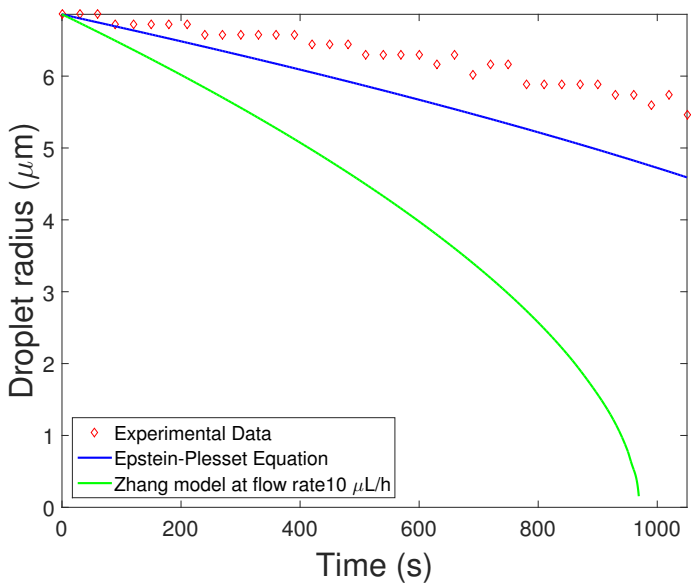

Figure 10: Dissolution of an undecanol microdroplet in water at 10 μM surfactant concentration

4 Oscillation Analysis of a Hydrodynamically Trapped Benzyl Benzoate Microdroplet

This section provides an oscillation analysis for a hydrodynamically trapped benzyl benzoate microdroplet at 10 $\mu L/h$. In the experiments the sampling period was 30 seconds. Figure 11 shows the position of a trapped microdroplet as a function of time.

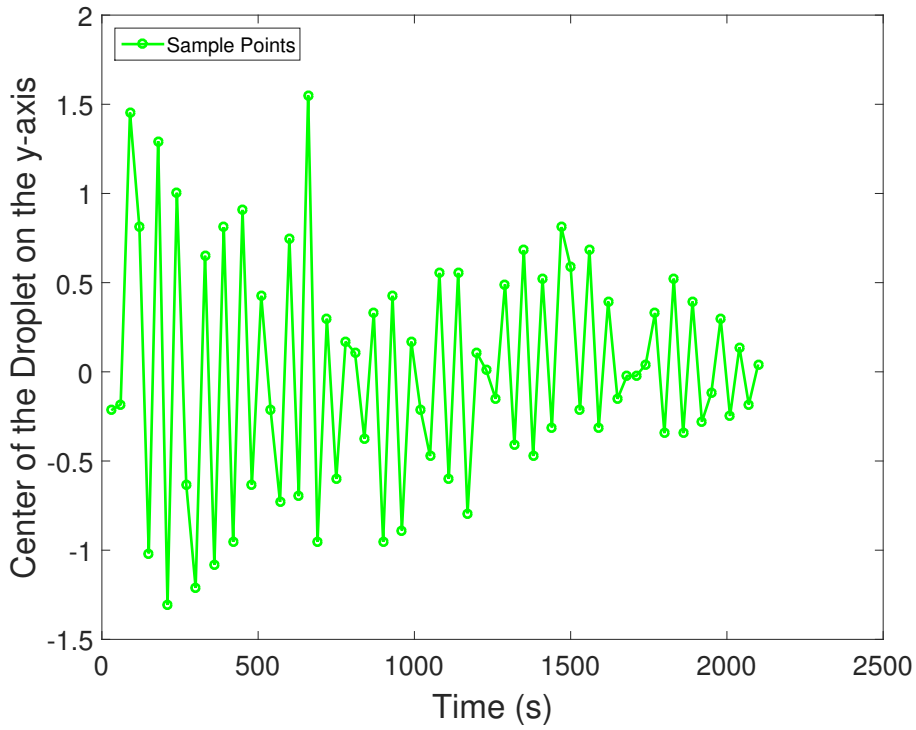

Figure 11: Position of a hydrodynamically trapped microdroplet on the y-axis.

Green circles indicate the sample points and green lines indicate the consecutive sample points. To analyze this data, we calculated the power spectral density of the position. Figure 12 reveals the dominant oscillation frequencies.

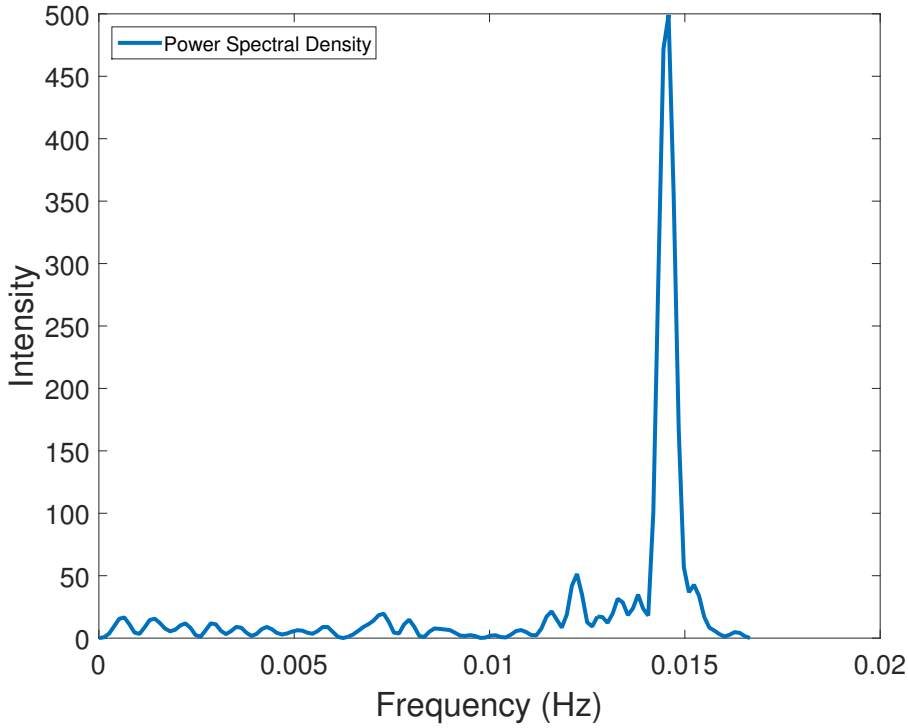

Figure 12: Power spectral density of the position on the y-axis of a hydrodynamically trapped microdroplet.

This graph indicates that the most distinct oscillation frequency is around 0.015 Hz meaning that oscillation period is around 66 seconds. This period might not be exact oscillation period since the sampling period is 30 and it is probably higher than the exact oscillation period. A trapped microdroplet oscillates because it is trapped at the unstable stagnation point and the feedback system tries to continuously adjust the position of the microdroplet. The oscillation amplitude decreases as a function of time since the mass of the trapped microdroplet decreases due to dissolution. To decrease the oscillation amplitude and frequency further, one should adjust the feedback parameters in the LabVIEW code.

5 Modelling

This section describes two models for the droplet dissolution in a simple extensional flow. The first model proposed by Epstein and Plesset [22] ignores the effects of the convection and so it is valid only for $Pe \to 0$, i.e., the diffusion dominates over the convection. The Peclet number defined as $Pe = UR/D$ where U , R and D are diffusion coefficient, droplet radius and the free stream velocity, respectively. The second model proposed by Zhang et al. [27] accounts for both diffusion and convection in a creeping flow regime and is based on the analytical solution obtained by Kurdyumov and Polyanin [26]. These models are first described in this section and than compared with the experimental data in the results and discussion section.

5.1 The Epstein-Plesset Model

Epstein-Plesset model was originally derived for dissolution of single gas bubbles in an infinite domain. Recently, Duncan and Needham [24] have shown that the Epstein-Plesset model also applies to dissolution of a single liquid droplets in a quiescent flow in an infinite domain. The model is briefly described here and the reader is referred to Ref. [22] for details.

Solution to diffusion problem for droplets starts with following assumptions. Assume that a droplet of initial radius R_0 is placed instantly in a quiescent fluid at time $t = 0$. Temperature and pressure of the host fluid are assumed to be constant. Initial concentration of dissolved droplet material in the host fluid is denoted by c_i and assumed to be uniform. Saturation concentration of the droplet fluid in the ambient host fluid is denoted by c_s. A cylindrical coordinate system

is placed at the center of the droplet and the dissolution is axisymmetric so that the droplet centroid remains fixed during the dissolution process. For a droplet of radius R and time $t \geq 0$, the dissolved droplet fluid concentration at a point $r \geq R$, where r is the radial distance between the center of bubble and the point where the concentration is sought, governed by the diffusion equation,

$$\frac{\partial c}{\partial t} = D\nabla^2 c. \tag{1}$$

In this equation, c and D denote the concentration and diffusion coefficient of the droplet fluid in the host fluid, respectively. Since the dissolution is assumed to be symmetric, the concentration only depends on the radial distance and time. Eq. (1) is solved with the following initial and boundary conditions:

$$c(r,0) = c_i,\ r \geq R;$$
$$\lim_{r\to\infty} c(r,t) = c_i,\ t \geq 0;$$
$$c(R,t) = c_s,\ t \geq 0.$$

To put the Eq. (1) in a familiar form, we introduce a dependent variable

$$u = r(c - c_s) \tag{2}$$

and replacing c with u, Eq. (1) becomes

$$\frac{\partial u}{\partial t} = D\left(\frac{\partial^2 u}{\partial r^2}\right) \tag{3}$$

with the following initial and boundary conditions

$$u(r,0) = r\delta$$

$$u(R,t) = 0$$

where $\delta = c_i - c_s$. One has to only make a linear shift in the r-coordinate by

$$\xi = r - R$$

in order to make the problem identical with a familiar problem in heat conduction which has the solution

$$u(r,t) = \frac{\delta}{(2\pi t)^{\frac{1}{2}}} \int_0^\infty (R+\xi') \left(exp(\frac{-(\xi-\xi')^2}{4Dt}) - exp(\frac{-(\xi+\xi')^2}{4Dt}) \right) d\xi'. \tag{4}$$

The concentration gradient at $r = R$ is directly found from Eq. (4)

$$\left(\frac{\partial u}{\partial r}\right)_R = \delta \left(1 + \frac{R}{(\pi D t)^{\frac{1}{2}}}\right). \tag{5}$$

Since $(\partial c/\partial r)|_R = (\partial u/\partial r)|_R/R$, one has

$$\left(\frac{\partial c}{\partial r}\right)_R = \delta \left(\frac{1}{R} + \frac{1}{(\pi D t)^{\frac{1}{2}}}\right). \tag{6}$$

Thus the mass transfer from the droplet into the ambient fluid is given by,

$$\frac{dm}{dt} = 4\pi R^2 D \left(\frac{\partial c}{\partial r}\right)_R. \tag{7}$$

Substituting Eq. (6) into Eq. (7) yields,

$$\frac{dm}{dt} = 4\pi R^2 D\delta\left(\frac{1}{R} + \frac{1}{(\pi Dt)^{\frac{1}{2}}}\right). \tag{8}$$

Using the following relation,

$$\frac{dm}{dt} = 4\pi R^2 \rho\left(\frac{dR}{dt}\right) \tag{9}$$

where ρ is the density of the droplet material, one obtains

$$\frac{dR}{dt} = -\frac{D(c_s - c_i)}{\rho}\left(\frac{1}{R} + \frac{1}{(\pi Dt)^{\frac{1}{2}}}\right). \tag{10}$$

This equation is integrated in time using MATLAB ODE45 routine. However, this model is only valid for diffusion dominated flows i.e. $Pe \ll 1$. To overcome this deficiency, we also use the Zhang model described in the following section.

5.2 The Kurdyumov-Polyanin-Zhang Model

In the microfluidic chip, microdroplets are trapped in a planar extensional creeping flow, and there is significant mass transfer due to convection. The transport problem for a spherical particle in an extensional flow was initially carried out by Gupalo and Riazantsev [28], and they treated the steady mass transfer from a sphere in the creeping fluid flow at high Peclet numbers. They solve the relevant problem in the approximation of diffusion boundary layer and their solution shows that Sherwood number, $Sh = KR/D$, where K is the mass transfer coefficient, is proportional to $Pe^{\frac{1}{3}}$ for a solid sphere and but to $Pe^{\frac{1}{2}}$ for a liquid drop.

Later, Bachelor [29] studied the mass transfer from a solid sphere suspended in a steady linear fluid flow and derived the analytical expressions for Sh at both small and large Pe. These are all analytical solutions and therefore restricted to the situation that Pe is either far larger or far smaller than the unity. It is difficult to obtain an analytical expression for the transfer rate at intermediate Pe. Kurdyumov and Polyanin solved mass transfer problem for spherical particles numerically in a linear Stokes shear flow and proposed approximate correlations for Sh at intermediate Pe based on asymptotic expansion of Sh given in analytical studies.

The problem definition in Kurdyumov paper starts as follows. Assume a spherical particle (drop or bubble) of radius a is placed in an axisymmetric linear shear flow. The concentration far from the spherical particle is denoted by C_∞. In the rectangular coordinate system denoted by $X_1,\ X_2,\ X_3$ which moves with the center of the drop, axisymmetric shear flow is described by the expressions

$$v_1 \to -EX_1,\ v_2 \to -EX_2,\ v_3 \to 2EX_3,\ R \to \infty \tag{11}$$

where $v_1,\ v_2,\ v_3$ are the fluid velocity components, E is the shear coefficient and $R = (X_1^2 + X_2^2 + X_3^2)^{\frac{1}{2}}$. Then the distribution of the concentration for diffusion from a spherical particle in a shear flow in the spherical coordinate system has the form

$$\frac{Pe}{sin\theta}\left(\frac{\partial\psi}{\partial\theta}\frac{\partial c}{\partial r} - \frac{\partial\psi}{\partial r}\frac{\partial c}{\partial\theta}\right) = \frac{\partial}{\partial r}\left(r^2\frac{\partial c}{\partial r}\right) + \frac{1}{sin\theta}\frac{\partial}{\partial\theta}\left(sin\theta\frac{\partial c}{\partial\theta}\right)$$

$$\psi = signE\left(r^3 - \frac{5\beta+2}{2\beta+2}\right) + \frac{3\beta}{2\beta+2}\frac{1}{r^2}sin^2\theta cos\theta,\ Pe = \frac{a^2|E|}{D} \tag{12}$$

with initial and boundary conditions

$$r = 1,\ c = 1;\ r \to \infty,\ c \to 0 \tag{13}$$

where $c = (C_\infty - C)/C_\infty$, C, $r = R/a$, β and ψ are dimensionless concentration, concentration, dimensionless radius, viscosity ratio of the drop to the surrounding fluid and dimensionless stream function, respectively. The Eq. (12) with conditions (13) was solved numerically on the interval $0 \leq \theta \leq \pi/2$ since the problem is symmetric about the plane $\theta = \pi/2$. For a bubble i.e. $\beta = 0$, the dominant terms of the asymptotic expansion of Sh at small and large Pe are

$$Sh = 1,\ Pe \to 0;\ Sh = (3Pe/\pi)^{\frac{1}{2}},\ Pe \to \infty. \tag{14}$$

Then, they provide Sh at intermediate Pe

$$Sh(0, Pe) = 0.6 + (0.16 + 0.96Pe)^{\frac{1}{2}} \tag{15}$$

which is consistent with the exact asymptotics (14). For a solid particle i.e. $\beta = \infty$, the dominant terms of the asymptotic expansion of Sh for a spherical particle in a shear flow at small and large Pe are

$$Sh = 1,\ Pe \to 0;\ Sh = 1.22Pe^{\frac{1}{3}},\ Pe \to \infty. \tag{16}$$

Then at intermediate Pe, they provide Sh

$$Sh(\infty, Pe) = 0.5 + (0.125 + 1.49Pe)^{\frac{1}{3}} \tag{17}$$

which is again consistent with the exact aysmptotics (16). For details reader is referred to [26]. Based on Eqs. (15,17), for a drop at intermediate Pe i.e. $0 \leq Pe \leq 100$, Sh is

$$Sh(\beta, Pe) = \frac{1}{\beta+1} Sh(0, Pe) + \frac{\beta}{\beta+1} Sh(\infty, Pe). \tag{18}$$

which is valid for the entire range of β numbers. The maximum Pe considered in this study is 2000 and also they only use a few numerical results to validate proposed approximate correlations. Later, it has been shown that these correlations with some modifications are valid for larger range of Peclet numbers for a spherical particle in Stokes velocity field at small Reynolds numbers by Zhang et al.[27] They validate the approximate correlations proposed by Zhang et al. by solving the convection diffusion equation using a finite difference method with the control volume formulation and using large number of numerical results. The flow field of simple extensional creeping flow of large extent for a fixed spherical drop is

$$\mathbf{u} = \mathbf{\Gamma} \cdot \mathbf{r} - \frac{\beta}{(\beta+1)r^5} \mathbf{E} \cdot \mathbf{r} - \left[\frac{5\beta+2}{2(\beta+1)} \frac{1}{r^5} - \frac{5\beta}{2(\beta+1)} \frac{1}{r^7} \times (\mathbf{r} \cdot \mathbf{E} \cdot \mathbf{r}) \mathbf{r} \right] \tag{19}$$

where $\mathbf{r}$, $\mathbf{\Gamma}$, $\mathbf{E}$ are the position vector, the transpose of the velocity gradient tensor, and the rate of strain tensor, respectively. For the particular geometry that a single

sphere of radius a immersed in a simple extensional creeping flow

$$\mathbf{\Gamma} = \mathbf{E} = \begin{pmatrix} -\frac{1}{2} & 0 & 0 \\ 0 & -\frac{1}{2} & 0 \\ 0 & 0 & 1 \end{pmatrix} E \tag{20}$$

where E characterizes the extension strength. Scaling Eq. (19) by $|E|a$, the flow velocity in dimensionless form in a spherical coordinate system, with the sphere center at the origin is

$$u_r = \left(1 - \frac{3}{2} sin^2\theta\right)\left(r - \frac{5\beta + 2}{2(\beta+1)r^2} + \frac{3\beta}{2(\beta+1)r^4}\right) \tag{21}$$

$$u_\theta = -\frac{3}{2} sin\theta cos\theta \left(r - \frac{\beta}{(\beta+1)r^4}\right) \tag{22}$$

$$u_\phi = 0. \tag{23}$$

The convection-diffusion equation is

$$\frac{\partial c}{\partial t} + \mathbf{u} \cdot \nabla c = D\nabla^2 c \tag{24}$$

where $\mathbf{u}$ is the velocity field. They solve Eq. (24) numerically under following assumptions. First, both the droplet and the host solution are Newtonian. Second, the shape of the particle remains spherical. Third, the physical properties including mass diffusivity, fluid viscosity, and density are constant and mass transfer does not affect flow structure. Then, the convection-diffusion equation for an axisymmetric mass transfer problem can be expressed in a spherical coordinate

system in the dimensionless form as

$$\frac{\partial C}{\partial \tau} + \frac{1}{r^2}\frac{\partial}{\partial r}(r^2 u_r C) + \frac{1}{r sin\theta}\frac{\partial}{\partial \theta}(u_\theta sin\theta C) = \frac{1}{Pe}\left[\frac{1}{r^2}\frac{\partial}{\partial r}\left(r^2\frac{\partial C}{\partial r}\right) + \frac{1}{r sin\theta}\frac{\partial}{\partial \theta}\left(\frac{1}{r} sin\theta \frac{\partial C}{\partial \theta}\right)\right] \tag{25}$$

where C and $\tau = |E|t$ are the dimensionless concentration and, the dimensionless time, respectively. The dimensionless concentration is defined by $C = (c - c_\infty)/(c^s - c_\infty)$, where c^s and c_∞ are saturation concentration of the ambient host fluid and concentration field far from the sphere. The initial and boundary conditions are

$$C = C^s = 1,\ r = 1;\ C = C_\infty = 0, r \to \infty. \tag{26}$$

One important result Zhang et al. confirm in their work is Sherwood number (18) provided by Kurdyumov and Polyanin at intermediate Pe is valid even though the proposed correlation derived from only a few numerical results. The other important result they prove is Sherwood number expression provided for liquid drop in simple extensional creeping flow at intermediate. Since Eq. (20) has half extension rate of Eq. (11), then Eq. (18) with half Pe can be written as

$$Sh(\beta, Pe) = \frac{1}{\beta+1}\Big\{0.6 + (0.16 + 0.48Pe)^{\frac{1}{2}} + \frac{\beta}{\beta+1}\Big\{0.5 + (0.125 + 0.745Pe)^{\frac{1}{3}}\Big\}. \tag{27}$$

which is even valid for larger Pe, i.e. $10 < Pe < 1000$. Also for the range $0 \leq Pe \leq 10$, Zhang et al. propose a more accurate correlation. For details reader

is referred to [27]. Thus mass transfer from the droplet into the ambient fluid is given by,

$$\frac{dm}{dt} = -K(c_s - c_i)A \tag{28}$$

where A is the surface area of the droplet. Substituting $m = (4/3)\pi r^3 \rho$ and $A = 4\pi r^2$, one obtains

$$\frac{d}{dt}\left(\frac{4}{3}\pi R^3 \rho\right) = -K(c_s - c_i)4\pi R^2. \tag{29}$$

Substituting K, from $Sh = KR/D$ into Eq. (29) and simplifying, one obtains

$$\frac{dR}{dt} = -D\frac{c_s - c_i}{R\rho}Sh. \tag{30}$$

Substituting Eq. (27) into Eq. (30), one obtains

$$\frac{dR}{dt} = -\frac{D(c_s - c_i)}{R\rho}\left(\frac{1}{\beta+1}\left\{0.6 + (0.16 + 0.48Pe)^{\frac{1}{2}}\right\} + \frac{\beta}{\beta+1}\left\{0.5 + (0.125 + 0.745Pe)^{\frac{1}{3}}\right\}\right). \tag{31}$$

This differential equation models the dissolution of a droplet in simple extensional creeping flow, therefore it is applicable to dissolution of hydrodynamically trapped microdroplets. To solve for $R(t)$, Eq. (31) is integrated in time using MATLAB ODE45 routine. This routine is provided in Appendix A.

6 Experimental Setup

The hydrodynamic trapping experimental setup consists of several main elements. These elements are a microfluidic chip, a 4-way valve, a pressure regulator, a gas tank, a camera, a microscope, a syringe pump and syringes, tubing, a computer running LabVIEW software. The framework of the overall experimental setup is in Figure 13.

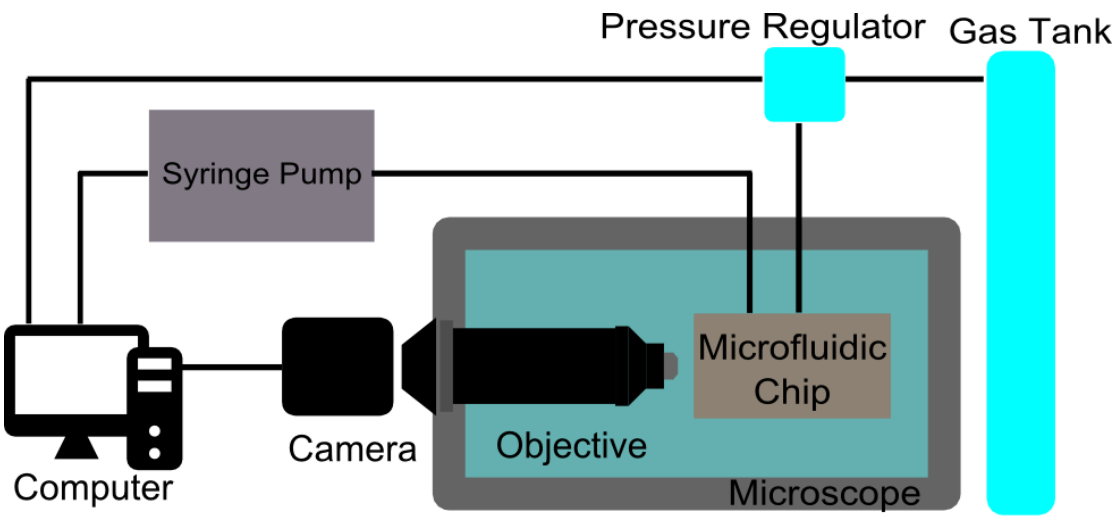

Figure 13: The framework of the hydrodynamic trap setup

Once the microdroplets are injected into the microfluidic chip, we run a home-built LabVIEW code in the controlling computer which runs the experimental setup automatically. Particles are observed with a high speed camera(Grasshopper3, Pointgrey) at 100 frames per second. When the microdroplets are in the trapping region, the LabVIEW code searches for particles with a predetermined radius size and if there is multiple droplets satisfying this condition, it picks the particle that is closest to the stagnation point. The LabVIEW code also determines the required pressure to keep the particle at the stagnation point and transmits required volt-

age signal to the pressure regulator(QVP1, Proportion Air). LabVIEW software is interfaced with the pressure regulator via a data acquisition card (NI-USB 6009). To keep the trapped microdroplet at the stagnation point, flow resistance in the outlet channels must be adjusted. This is done by applying appropriate amount of pressure to the pneumatic membrane valve that is atop the lower outlet channel. The applied pressure ranges from 0-12 psi. We use a standard gas tank at 200 psi filled with nitrogen to supply pressure to the pressure regulator. The host and sample fluids are inject into the microfluidic chip with a syringe pump (Phd Ultra, Harvard Apparatus). Typical flow rates range from 5 μl/h to 40 μl/h. Syringe pump is interfaced with a computer and we can set the flow rates using the LabVIEW code. Two syringes(1750-ttl, Hamilton), one for sample fluid and the other one for host fluid, is mounted on the syringe pump. Both of them were 500 μl syringes. Syringes and microfluidic chip are connected through PTFE tubing. There is 4-way valve(Western Analytical Products) in between the sample fluid syringe and the microfluidic chip enabling us to turn on or off the sample fluid.

6.1 Microfluidic Chip and Fabrication

The most essential part of the experimental setup is microfluidic chip. Throughout the course of experiments, we have arrived to a final chip layout. Design of this layout is performed in a vector graphic design software (Adobe Illustrator). Figure 14 illustrates the layout of our final design for the microfluidic chip.

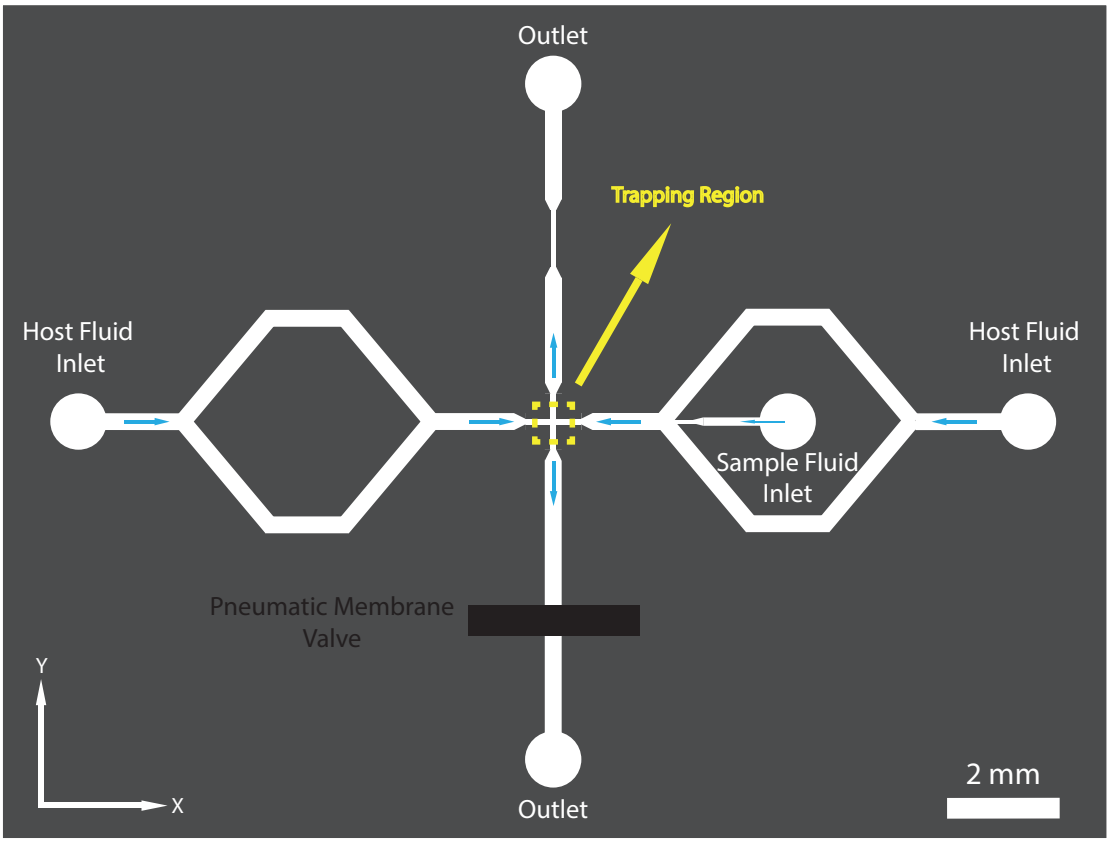

Figure 14: Layout of the microfluidic chip

In the design, there are 5 connection ports indicated as white circles at the edges of the chip. White color indicates the microfluidic channels and channel width is 300 μm. Three of them are fluid inlets which are located on the x axis and remaining two are fluid outlets which are located on the y axis. Trapping region is indicated with a dashed yellow square at the center of the chip. The microdroplet comes from sample inlet and reaches to trapping region and is trapped along y axis. At the trapping region channel width is 150 μm. Thickness of the fluidic channel is 40 μm. Along the upper half of the channel on the y axis, there is a constriction with a width of 150 μm. The constriction is used to increase flow resistance.

By doing so, the flow is inclined to exit from the lower outlet channel since this channel has lower resistance than the upper one. To control flow resistance in the lower outlet channel, there is a pneumatic membrane valve indicated by the horizontal black band. By applying pressure on the pneumatic membrane valve, we can actively adjust the position of the stagnation point and also the position of the trapped microdroplet. A sample trapped microdroplet in the microfluidic chip using hydrodynamic trapping is shown in Figure (15). Arrows indicate the flow direction in each channel.

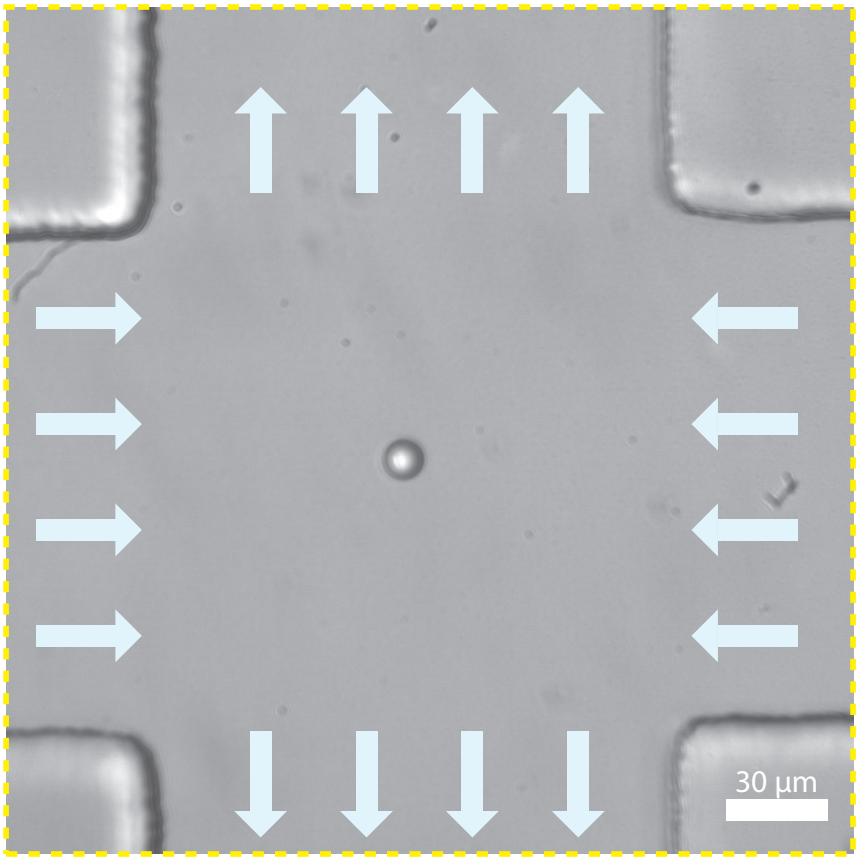

Figure 15: A hydrodynamically trapped benzyl benzoate droplet in extensional flow

The pneumatic valve is one of the most important part of the microfluidic

chip. It is on the control layer of the chip and is 150 μm thick. When gas pressure is applied, it deflects downwards on an outlet channel and increases the flow resistance. Due to up and down movement of the pneumatic valve, the position of the stagnation point can be controlled in real-time. Figure 16 illustrates the working principle of the valve.

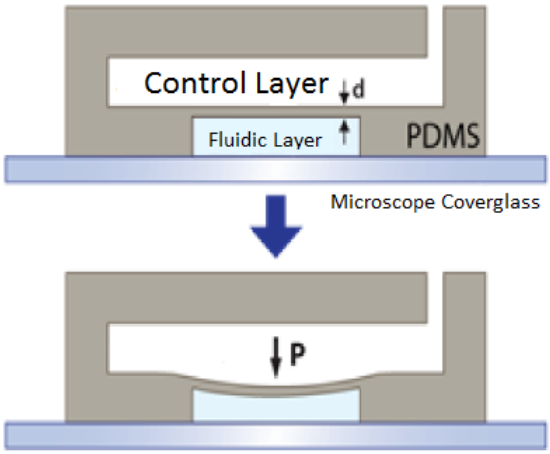

Figure 16: Pneumatic membrane valve showing the effect of applied pressure.

6.2 Experimental Setup for Dye Lasing in Hydrodynamically Trapped Microdroplets

After trapping a microdroplet, the lasing experiments are performed with the following experimental setup. Here, the main components are a Q-switched laser, a shutter, a monochromator, a spectroscopic CCD, a control PC, a microscope objective, mirrors and lenses. Figure 17 shows the main elements of the experimental setup.

We optically pump a dye doped microdroplet with a Q-swithed $NY : YVO_4$ laser at 532 nm and the laser beam goes through a shutter and a polarizing beam

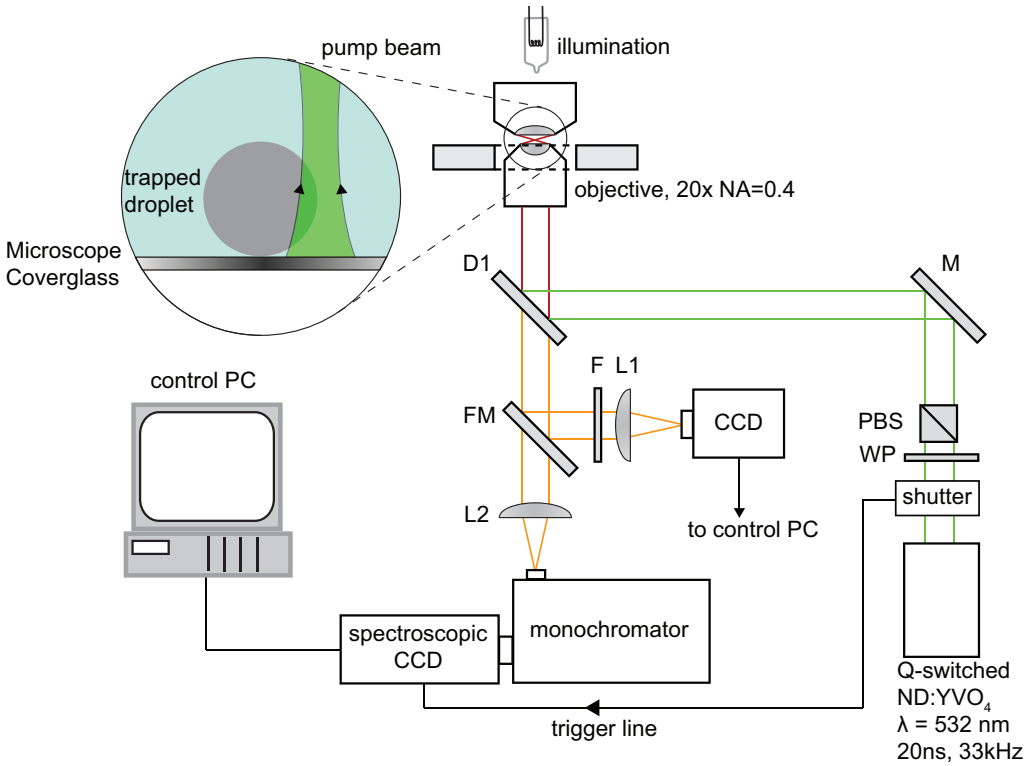

Figure 17: Experimental setup for dye lasing.

splitter. After exciting the droplet from the surface, the emission signal of the dye is collected with the same microscope objective and reaches to the monochromator. Spectral information is generated by the spectroscopic CCD camera.

6.3 Microdroplet Generation and Injection

Microdroplets made of various materials are used in the experiments. These droplets have various radii. To generate droplets, we put small amount of droplet liquid into a glass vial filled with DI water at a certain amount of surfactant concentration. After capping the vial, we shake the vial thoroughly so that bulk droplet liquid turns into microdroplets. In the experiments, we used DSS surfac-

tant (Docusate Sodium Salt, Sigma Aldrich) in DI water and the concentration of the surfactant was either 10 μM or 10 mM. These values are determined experimentally to ensure stable microdroplets within the host fluid. Surfactant is important for both stabilizing droplets and for generating a boundary layer on droplets thus preventing sticking of droplets to PDMS or microscope slide. We incubate the vial overnight to obtain a saturated emulsion with stable microdroplets. We call this solution as sample fluid. Droplet materials have different densities than water hence before withdrawing sample fluid from the vial, gently shake the vial once more before taking out the sample fluid in order to have sufficient amount of droplets in the sample syringe.

6.4 Image Analysis

Measuring droplet radius is essential, since in this work, we performed experimental studies and modeled change in droplet radius as a function of time. After taking a series of snapshots, usually one image per 30 seconds, via camera (PointGrey, Grasshopper3) using LabVIEW, images are analyzed in ImageJ. This software finds the bounding box of the trapped particle in units of pixels where pixels are converted into real distance by multiplying by a scalar.

6.5 Physical Properties of the Materials

In the dissolution experiments, we used four different droplet materials with known diffusion coefficients and saturation concentrations in water. Three alcohols n-octanol, n-decanol and undecanol are chosen since they have relatively low saturation concentration and their diffusion coefficient are known from the literature.

Table 1 summarizes material properties of the materials used in the experiments. We also used benzyl benzoate in the experiments.

Material Name	Diffusion Coefficient (m^2/s)	Saturation Concentration (kg/m^3)	Density (kg/m^3)	Viscosity (cP)	Refractive Index
n-Octanol	0.652×10^{-9}	0.54	0.824	6.24	1.429
n-Decanol	0.613×10^{-9}	0.037	0.829	12.048	1.437
Undecanol	0.535×10^{-9}	0.019	0.829	17.2	1.442
BB	0.539×10^{-9}	0.015	1.118	8.292	1.568

Table 1: Materials used in the experiments; three alcohols and benzyl benzoate with measured saturation concentrations and calculated diffusion coefficients.

7 Conclusion & Discussion

In this thesis, first, we report lasing from hydroynamically manipulated dye doped benzyl benzoate microdroplets. Previously lasing from optically manipulated dye doped microdroplets has been shown and this study extends it to hydrodynamic trap case. This novel technique also allowed us to take lasing spectra from the same trapped microdroplet at a position. The consecutive spectra of a dye doped microdroplet showed shift in all lasing modes to shorter wavelengths indicating a change in the size of the droplet. From then on, we observed the dissolution of microdroplets in water medium and proposed an equation from the literature modelling the dissolution of liquid microdroplets. Some materials showed good consistency with the model but some didn't.

We provided an explanation for the difference between the observed experimental results and the theoretical model. One possible reason might be the difference between the observed and reported values of solubility. The other possibility is the inconsistency in coefficient of diffusion. In the literature most diffusion coefficients are provided as calculated values based on a theoretical model, which may not accurately reflect the actual diffusion coefficients. As indicated, alcohols are much more sensitive to surfactant concentration than benzyl benzoate. But the model doesn't include the concentration of surfactant. The type and concentration of surfactant remains an important parameter for controlling dissolution, even at low concentrations used in our experiments (as low as 10 μM). The microfluidic chips might be causing a deviation in our results, since droplets have a long way to travel to reach the stagnation point, due to low surfactant concentration, they stick to the channels. Even though we turn the sample fluid off, the stuck droplets

in channels could increase the concentration of the ambient host fluid therefore causing longer dissolution times than anticipated. The last component causing error is the position of the dissolving microdroplet in the microfluidic chip. The theory assumes a droplet dissolving in simple extensional extensional flow without any boundary conditions but in the microfluidic chip, since droplet material has a different density than water, the trapped droplet either sits on the floor or on the ceiling and the contact part of the droplet does not experience any dissolution.

8 Appendix A

```
function f=EP_Oguz(t,r)

% define Epstein-Plesset Model Parameters
% kappa = diffusion coefficient [m^2/s]
% cs = saturation concentration [kg/m^3]
% ci = initial concentration [kg/m^3]
% rho = density of material [kg/m^3]

global kappa
global cs
global ci
global rho

f = -kappa*(cs-ci)*(1/rho)*(1/r + 1/sqrt(pi*kappa*t));
```

```
function f_ep_modified=EP_Modified_Oguz(t,r)

% Define modified Epstein-Plesset Equation parameters
% kappa = diffusion coefficient [kg/m^3]
% cs = saturation concentration [kg/m^3]
% ci = initial concentration [kg/m^3]
% rho = density of material [kg/m^3]
% vd = viscosity of droplet [kg/s*m]
% vs = viscosity of surroundins [kg/s*m]
% lambda = viscosity ratio vd/vs
% fr = flow rate [m^3/s]
% width = width of the channel [m]
% height = height of the channel [m]
% area [m^2]
% fsv = free stream velocity [m/s]
% pe = fsv*r/kappa;
% A = kappa*(cs-ci)/(rho*r);
% B = (1/lambda)*(0.6 + (0.16+0.48*pe)^(1/2));
% C = (lambda/(1+lambda))*(0.5 + (0.125 + 0.745*pe)^(1/3));
% sh = B + C; (sherwood number)

global kappa cs ci rho lambda fsv


% calculate peclet number for each time instant
pe = fsv*r/kappa;
A = kappa*(cs-ci)/(rho*r);
```

```
B = (1/lambda)*(0.6 + (0.16+0.48*pe)^(1/2));
C = (lambda/(1+lambda))*(0.5 + (0.125 + 0.745*pe)^(1/3));
sh = B + C;
f_ep_modified = -A*sh;
```

```
% This scripts solves both Epstein-Plesset equation
% and Zhang et.al. Equation for a defined material.
% Plots, experimental data, EP equation and Zhang model
% Written by Oguz Kayillioglu
% Date: May 18, 2015
%%%%%%%%%%%%%%%%%%%%%%%%%%%%%%%%%%%%%%%%%%%%%%%%%%%%%%%%%%%%
clc
clear all
close all

% define measurement date
date = ' June 05, 2015';

% define material name
material_name = ' Benzyl Benzoate';

% define graphic name
C_DSS = ' 10 uM DSS ';
graph = 'Graph for ';
graphic_name= strcat(graph,C_DSS, material_name,date);

% frs = flow rate scaler [ul/h]
% ic = initial concentration [%]
frs = 10;
ic = 0;

% load ImageJ outputted excel file
filename=['C:\Users\okayillioglu\Desktop\'...
    'code result\bb\Results_June05_2015_20ul_BB1.xlsx'];

num = xlsread (filename);
time = num(:,10);
rad = num(:,9)*10^-6;
r0 = rad(1);

%%%%%%%%%%%%%%%%%%%%%%%%%%%%%%%%%%%%%%%%%%%%%%%%%%%%%%%%%%%%
% plot experimental data
figure
plot (time,rad,'rd');
hold on

%%%%%%%%%%%%%%%%%%%%%%%%%%%%%%%%%%%%%%%%%%%%%%%%%%%%%%%%%%%%
```

```
% solves EP model using ordinary differantial equation solver
% define ode45 parameters
% t0 = initial time of ode
% stepsize
% define initial droplet diameter
t0 = 0.1 ;
stepsize = 0.1;
tfinal = time(end);


% define global variables for epstein-plesset model
% kappa = diffusion coefficient [m^2/s]
% cs = saturation concentration of solute in water [kg/m^3]
% ci = initial concentration of solute in water [kg/m^3]
% density of solute [kg/m^3]

global kappa cs ci rho
kappa = 0.539*10^-9;
cs =  15.39*10^-3;
ci = cs*(ic/100);
rho = 1118;

%%%
```

```
fsv = fr/area;

%%%
```

References

[1] N. T. Nguyen and Z. Wu. *J. Micromech. Microeng.* **15**.2 (2005).

[2] V. Hessel, H. Löwe, and F. Schönfeld. *Chem. Eng. Sci.* **60**.8 (2005).

[3] D. E. Angelescu and D. Siess. *Sensors, 2005 IEEE.* IEEE. 2005.

[4] D. R. Gossett, W. M. Weaver, A. J. Mach, S. C. Hur, H. T. K. Tse, W. Lee, H. Amini, and D. Di Carlo. *Anal. Bioanal.Chem.* **397**.8 (2010).

[5] D. Kohlheyer, J. C. T. Eijkel, A. van den Berg, and R. Schasfoort. *Electrophoresis* **29**.5 (2008).

[6] S. Y. Teh, R. Lin, L. H. Hung, and A. P. Lee. *Lab Chip* **8**.2 (2008).

[7] C. Zhang, J. Xu, W. Ma, and W. Zheng. *Biotechnol. Adv.* **24**.3 (2006).

[8] R. M. Johann. *Anal. Bioanal. Chem.* **385**.3 (2006).

[9] J. Nilsson, M. Evander, B. Hammarström, and T. Laurell. *Anal. Chim. Acta* **649**.2 (2009).

[10] C. Yi, C. Li, S. Ji, and M. Yang. *Anal. Chim. Acta* **560**.1 (2006).

[11] M. Tanyeri, J. Chavarria, Eric M., and C. M. Schroeder. *Appl. Phys. Lett.* **96**.22 (2010).

[12] M. Tanyeri, M. Ranka, N. Sittipolkul, and C. M. Schroeder. *Lab Chip* **11**.10 (2011).

[13] M. Tanyeri and C. M. Schroeder. *Nano Lett.* **13**.6 (2013).

[14] M. Aas, A. Jonáš, and A. Kiraz. *Opt. Commun.* **290** (2013).

[15] R. S. Harland, A. Gazzaniga, M. E. Sangalli, P. Colombo, and N. A. Peppas. *Pharm. Res.* **5**.8 (1988).

[16] P. B. O'Donnell and J. W. McGinity. *Adv. Drug Delivery Rev.* **28**.1 (1997).

[17] G. Taylor. *Proceedings of the Royal Society of London A: Mathematical, Physical and Engineering Sciences.* **219**. 1137. The Royal Society. 1953.

[18] R. Aris. *Proc. R. Soc. London, Ser. A.* **235**. 1200. The Royal Society. 1956.

[19] E. L. Cussler. Cambridge University Press, 2009.

[20] H. M. Baranowska and K. J. Olszewski. *BBA-Gen. Subjects* **1289**.3 (1996).

[21] F. Loureiro, B. Neto, C. S. Moreira, Antonio M. N. Lima, and H. Neff. *Sens. Actuators, B* **154**.2 (2011).

[22] P. S. Epstein and M. S. Plesset. *J. Chem. Phys.* **18**.11 (1950).

[23] P. B. Duncan and D. Needham. *Langmuir* **20**.7 (2004).

[24] P. B. Duncan and D. Needham. *Langmuir* **22**.9 (2006).

[25] J. T. Su and D. Needham. *Langmuir* **29**.44 (2013).

[26] V. N. Kurdyumov and A. D. Polyanin. *Fluid Dyn.* **25**.4 (1990).

[27] J. Zhang, C. Yang, and Z.S. Mao. *AlChE J.* **58**.10 (2012).

[28] P. Gupalo and S. Riazantsev. *J. Appl. Math. Mech.* **36**.3 (1972).

[29] G.K. Batchelor. *J. Fluid Mech.* **95**.02 (1979).